Investigation on sensitivity enhancement for optical fiber speckle sensors

Sen QIAN,[1] Yang XU,[1,3] Lisheng ZHONG,[1] and Lei SU[2,4]

[1]*State Key Laboratory of Electrical Insulation and Power Equipment, Xi'an Jiaotong University, Xi'an, China*
[2]*School of Engineering and Materials Science, Queen Mary University of London, E1 4NS, London, United Kingdom*
[3]*xuyang@mail.xjtu.edu.cn*
[4]*l.su@qmul.ac.uk*

Abstract: We present a detailed theoretical and experimental study on the sensitivity enhancement for multimode fiber (MMF) speckle sensor. Using mode coupling theory, we derive an expression showing that the sensitivity of the MMF speckle sensor depends on the intensity profile of the MMF modes. Particularly, we use our theory to study the influence of the spatial filtering window on the sensitivity, and the experimental results have found a good agreement with the theory. Our results suggest that the sensitivity of an MMF speckle sensor can be greatly enhanced by adjusting the size and location of the spatial filtering window. An 80-fold improvement on sensitivity was achieved in our experiment, as compared with the conventional MMF speckle sensor with the filtering window placed at the center of the speckle field.

References and links

1. J. W. Goodman, Speckle Phenomena in Optics:Theory and Applications(Roberts and Company Publishers, 2010), Chap.7.
2. Y. Wang, H. Cai, R. Qu, Z. Fang, E. Marin, and J.P. Meunier, "Specklegram in a grapefruit fiber and its response to external mechanical disturbance in a single-multiple-single mode fiber structure," Appl. Opt. 47(20), 3543–3548 (2008).
3. J. A. Gómez and A. Salazar, "Self-correlation fiber specklegram sensor using volume characteristics of speckle
4. patterns," Opt. Lasers Eng. 50(5), 812–815 (2012).
5. L. Rodriguez-Cobo, M. Lomer, A. Cobo, and J. Lopez-Higuera, "Optical fiber strain sensor with extended
6. dynamic range based on specklegrams," Sensor Actuat. A 203, 341–345 (2013).
7. T. A. Eftimov, W. J. Bock, P.E. Balzhiev, V. M. Plachkova, and K. Zhelyazkova, "Securitized optical fiber communication and sensor systems using mode-selective couplers," J. Lightwave Technol. 32(21), 3345–3355 (2014).
8. J. Li, H. Cai, J. Geng, R. Qu, and Z. Fang, "Specklegram in a multiple-mode fiber and its dependence on longitudinal modes of the laser source," Appl. Opt. 46(17), 3572–3578 (2007).
9. L. V. Amitonova, A. P. Mosk, and P. W. H. Pinkse, "Rotational memory effect of a multimode fiber," Opt. Express 23(16), 20569–20575 (2015).
10. M. Matsuura, R. Furukawa, Y. Matsumoto, A. Inoue, and Y. Koike, "Evaluation of modal noise in graded-index silica and plastic optical fiber links for radio over multimode fiber systems," Opt. Express 22(6), 6562–6568 (2014).
11. L. Rodriguez-Cobo, M. Lomer, A. Cobo, and J. Lopez-Higuera, "Radial processing scheme of speckle patterns for sensing applications," in *Advanced Photonics Congress 2013*, OSA Technical Digest (Optical Society of America, 2013), paper JT3A.26.
12. W.B. Spillman, B.R. Kline, L.B. Maurice, and P.L. Fuhr, "Statistical mode sensor for fiber optic vibration sensing uses," Appl. Opt. **28**(15), 3166-3176 (1989).
13. A. Malki, R. Gafsi, L. Michel, M. Labarrere, and P. Lecoy, "Impact and vibration detection in composite materials by using intermodal interference in multimode optical fibers," Appl. Opt. **35**(25), 5198-5201 (1996).
14. N. Gomez, and J. Gomez, "Effects of the speckle size on non-holographic fiber specklegram sensors," Opt. Laser Eng. **51**(11), 1291-1295 (2013).
15. K. Pan, C. Uang, F. Cheng, and F. Yu, "Multimode fiber sensing by using mean-absolute speckle intensity variation," Appl. Opt. **33**(10), 2095-2098 (1994).
16. L. Rodriguez-Cobo, M. Lomer, and J.M. Lopez-Higuera, "Fiber specklegram-multiplexed sensor," J. Lightwave Technol. **33**(12), 2591-2597 (2015).

17. F. Yu, M. Wen, S. Yin, and C. Uang, "Submicrometer displacement sensing using inner product multimode fiber speckle fields," Appl. Opt. **32**(25), 4685-4689 (1993).
18. P. Podbreznik, D. Donlagic, D. Lesnik, B. Cigale, and D. Zazula, "Cost-efficient speckle interferometry with plastic optical fiber for unobtrusive monitoring of human vital signs," J. Biomed. Opt. **18**(10), 107001-1-107001-8 (2013).
19. X. Xu, W.B. Spillman, R.O. Claus, K.E. Meissner, and K. Chen, "Spatially distributed sensor with dual processed outputs," Proc. SPIE **5855**, 58-61 (2005)
20. Y. Dong, P. Xu, H. Zhang, Z. Lu, L. Chen, and X. Bao, "Characterization of evolution of mode coupling in a graded-index polymer optical fiber by using Brillouin optical time-domain analysis," Opt. Express **22**(22), 26510-26516 (2014).
21. L. Rodriguez-Cobo, M. Lomer, and J. Lopez-Higuera, "Common frequency suppression method for fiber specklegram perimeter sensors," Proc. SPIE **9634**, 96343R-2 (2015).
22. L. Rodriguez-Cobo, M. Lomer, and J. Lopez-Higuera, "Fiber specklegram sensors sensitivities at high temperatures," Proc. SPIE **9634**, 96347J-1 (2015).
23. D. Gloge, "Optical power flow in multimode fibers," Bell Syst. Tech. J. **51**(8), 1767-1783 (1972).
24. C.P. Tsekrekos, R.W. Smink, B.P. de Hon, A.G. Tijhuis, and A.M.G. Koonen, "Near-field intensity pattern at the output of silica-based graded-index multimode fibers under selective excitation with a single mode fiber," Opt. Express **15**(7), 3656-3664 (2007).
25. B. Huang, N.K. Fontaine, R. Ryf, B. Guan, S. Leon-Saval, R. Shubochkin, Y. Sun, R. Lingle Jr, and G. Li, "All-fiber mode-group-selective photonic lantern using graded-index multimode fibers," Opt. Express **23**(1), 224-234 (2015).
26. W. Ha, S. Lee, Y. Jung, J.K. Kim, and K. Oh, "Acousto-optic control of speckle contrast in multimode fibers with a cylindrical piezoelectric transducer oscillating in the radial direction," Opt. Express **17**(20), 17536–17546 (2009).
27. P.J. Kajenski, P.L. Fuhr, and D.R. Huston, "Mode coupling and phase modulation in vibrating waveguides," J.Lightwave Technol. **10**(9), 1297-1301 (1992).
28. D. Marcuse, *Theory of Dielectric Optical Waveguides* (Academic, 1991), Chap.4.
29. L. Su, K.S. Chiang, and C. Lu, "CO2-laser-induced long-period gratings in graded-index multimode fibers for sensor applications," IEEE Photon. Technol. Lett. **18**(1), 190-192 (2006).
30. A.F. Garito, J. Wang, R. Gao, "Effects of random perturbations in plastic optical fibers," Science **281**(14), 962-967 (1998).
31. S. Savovic, A. Djordjevich, "Mode coupling in strained and unstrained step-index plastic optical fibers," Appl. Opt. **45**(26), 6775-6780 (2006)
32. S Savovic, M. Kovacevic, J. Bajic, D. Stupar, A. Djordjevich, M. Zivanov, B. Drljaca, A. Simovic, and K. Oh, "Temperature dependence of mode coupling in low NA plastic optical fibers," J. Lightwave Technol. **33**(1), 89-94 (2015).
33. D.A. Boas, and A.K. Dunn, "Laser speckle contrast imaging in biomedical optics," J. Biomed. Opt. **15**(1), 011109-1-011109-12 (2010).
34. J. Qiu, Y. Li, Q. Huang, Y. Wang, and P. Li, "Correcting speckle contrast at small speckle size to enhance signal to noise ratio for laser speckle contrast imaging," Opt. Express **21**(23), 28902-28913 (2013).
35. A. Lev, and B. Sfez, "Acousto-optical detection of hidden objects via speckle based imaging," Opt. Express **23**(20), 26460-26471 (2015).

1. Introduction

The multimode fiber (MMF) speckle pattern, consisting of many granular bright spots, is formed as a result of interference between the modes propagating within the optical fiber [1]. This MMF speckle field is sensitive to external perturbations, and therefore is excellent in measuring a number of parameters [2-7]. MMF speckle sensors offer many advantages such as large coupling tolerance, easy installation and implementation of low-cost optoelectronics [8].

MMF speckle pattern varies if the MMF is perturbed, although the total intensity of the speckle field is approximately a constant because of the conservation of light propagating within the fiber. The speckle pattern variation serves as the principle for optical fiber speckle sensors [9]. Several methods have been proposed to measure the speckle variation. One commonly used method is the spatial filtering, which monitors a section of the MMF speckle field [1,5,6,10-12]. For example, a pinhole can be placed in front of the photo-detector, only allowing the selected section of the speckle field to pass through to the photo-detector [10]. Alternatively, a single mode fiber (SMF) can be spliced to the MMF to effectively serve as a spatial filter [12]. Other methods, including the mean absolute speckle intensity variation method [10,13,14] and the intensity inner product method, were also used [15].

As a widely used and successfully commercialized fiber-optic sensing technology, MMF speckle sensing has been continuously developed over the past and have found many real applications, such as heartbeat monitoring or embedded sensing in a smart bed [16,17]. There are still strong ongoing research efforts mainly to improve the speckle sensor performance. A suitable model to interpret the speckle-pattern variation under perturbation is desirable but very challenging to be developed due to the various factors influencing the speckle pattern [14]. For example, the misalignment between the lead-in pigtail optical fiber and the MMF can affect the speckle distribution [8,18]. The light source also influences the sensitivity. For example, a light source with higher coherence generally shows a speckle pattern of higher contrast and better sensitivity [14]. In addition, the coherence length of the light source needs to be tailored when the speckle sensor is designed for long distance applications [19]. Moreover, the number of modes supported by the MMF affects the speckle pattern and the sensitivity. A larger number of modes lead to higher sensitivity [20]. Furthermore, the sensitivity of the speckle sensor depends on the properties of the detector too. Three main characteristics of a detector are usually considered, namely, the resolution, the sensor area and the dynamic range [14]. However, there are few studies on the influence of spatial modes on the sensor performance. We expect this effect to be significant, because different spatial modes should respond to external perturbations quite differently. Therefore, by selecting a specific spatial filtering window to detect certain spatial mode groups, the sensitivity could be improved. In this study, we firstly derive a theoretical formula showing how the spatial filtering window can be selected to improve the sensitivity of the speckle sensor. Then, we verify the simulation results using experiments.

2. Theory

In MMFs, the $LP_{l,v}$ fiber modes can degenerate to cylindrical modes, which are also called the principal mode groups (PMG) with a new subscript $m=l+2v$ [21-23]. The transverse wavenumbers and propagation constants within the same PMG are similar to each other in value. Thus, for a step-index MMF, each cylindrical mode should correspond to a spatial ring in the MMF output image plane [21]. When the MMF is perturbed, the mode coupling occurs, and the following coupled equation [21,24-27] is used to describe the mode coupling:

$$\Delta P_m = \sum\nolimits_{n=1\&n\neq m}^{N} d_{mn}(P_n - P_m) \tag{1}$$

where d_{mn} is the coupling coefficient between the mth and nth guided mode, P_m and P_n are the initial powers of mth and nth mode, and N is the total number of guided modes. Another attenuation factor should also be included in Eq. (1) if the attenuation needs to be considered [28-30]. Eq. (1) shows the total power variation of the mth mode through mode coupling from the power of all the other modes. Given that the mode coupling is dominated between the neighboring modes [21,27-30], Eq. (1) can be simplified as:

$$\Delta P_m = d_m(P_{m+1} - P_m) + d_{m-1}(P_{m-1} - P_m) \tag{2}$$

where only the mode coupling between neighboring modes is taken into account.

Since coupling dominates between neighboring cylindrical modes and each mode corresponds to a spatial ring in the image plane, the power exchange in the image plane also dominates between neighboring rings (or modes). An example is shown in Fig 1. Supposing that the spatial filtering window only allows the rings P_1, P_2, P_3, P_4, P_5, and P_6 to be detected, the power of each ring can be derived using following equations based on Eq. (2):

$$P_1(t+\Delta t) = P_1(t) + (P_0 - P_1)\chi_{01} - (P_1 - P_2)\chi_{12} \tag{3}$$

$$P_2(t+\Delta t) = P_2(t) + (P_1 - P_2)\chi_{12} - (P_2 - P_3)\chi_{23} \tag{4}$$

$$P_3(t+\Delta t) = P_3(t) + (P_2 - P_3)\chi_{23} - (P_3 - P_4)\chi_{34} \tag{5}$$

$$P_4(t+\Delta t) = P_4(t) + (P_3 - P_4)\chi_{34} - (P_4 - P_5)\chi_{45} \tag{6}$$

$$P_5(t+\Delta t) = P_5(t) + (P_4 - P_5)\chi_{45} - (P_5 - P_6)\chi_{56} \tag{7}$$

$$P_6(t+\Delta t) = P_6(t) + (P_5 - P_6)\chi_{56} - (P_6 - P_7)\chi_{67} \tag{8}$$

where the χ_{ij} represents the power exchange coefficients between the *i*th and the *j*th rings. The meaning of the above equations can be easily understood. For example in Eq. (3), the power change on P_1 equals to the net power flow into the ring, i.e. the power flowing into the ring minus the power flowing out of the ring.

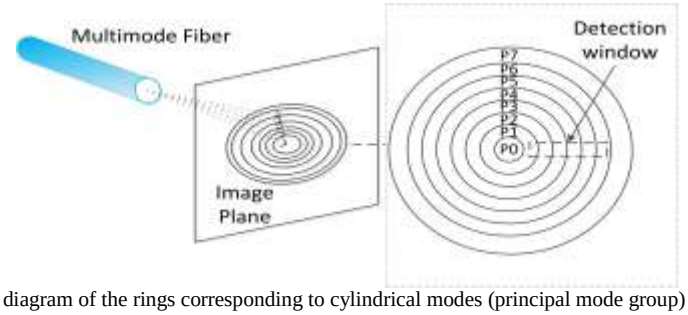

Fig. 1. Schematic diagram of the rings corresponding to cylindrical modes (principal mode group) in the image plane

The power detected by the window is the summation of Equations (3)-(8):

$$\begin{aligned} P_{window}(t+\Delta t) &= \alpha P_1(t+\Delta t) + \sum_{i=2}^{i=5} P_i(t+\Delta t) + \beta P_6(t+\Delta t) \\ &= P_{window}(t) + \alpha\Delta_{01}\chi_{01} + (1-\alpha)\Delta_{12}\chi_{12} - (1-\beta)\Delta_{56}\chi_{56} - \beta\Delta_{67}\chi_{67} \end{aligned} \tag{9}$$

where Δ_{ij} represents the power difference between the *i*th and *j*th rings. The coefficients α and β are introduced because the rings P_1 and P_6 are only partially covered by the window. Since the mode coupling coefficient d_{mn} is a function of external perturbation, it is expected that the power exchange coefficient χ_{mn} is also a function of external perturbation. If we assume a uniform power exchange coefficient χ, Eq. (9) can be expressed as:

$$P_{window}(t+\Delta t) = P_{window}(t) + (\alpha\Delta_{01} + (1-\alpha)\Delta_{12} - (1-\beta)\Delta_{56} - \beta\Delta_{67})\chi \tag{10}$$

A dynamic signal can be detected by the window if the second term of Eq. (10) is not zero, i.e. there is net power exchange to the window. Otherwise, the power detected through the window remains as a constant over time. The coefficient χ is determined by two factors, namely, the inherent deformation and applied deformation [25,26]. In Eq. (10), a large coefficient of χ will result in a strong power variation. This suggests that the sensing signal very much depends on the mode power difference at the edge of the window, $\Delta_{(i)(i+1)}$. It should be noted that Eq. (10) can be extended to an arbitrary window covering any number of rings. An important conclusion can be drawn here: the net power exchange at the edge of the filtering window contributes to the dynamic sensing signal, which further determines the sensitivity.

The sensitivity of the speckle sensor, related to the detected signal amplitude, with a flat-top intensity distribution is shown in Fig. 2. The circles in the blue curve represent the spatial rings in the image plane. The sensitivities of windows covering 4 and 12 rings were calculated according to Eq. (10). Because we assumed that the detection window completely covered the edge rings, the values of α and β, which represented the coverage ratio of the edge rings by the

window, were set to 1. Then, the power difference Δ at both edge rings were calculated, and the differences between these two were used to represent the sensitivity. It can be seen clearly that both the location and the size of the window affect the sensitivity of the speckle sensor. For a small window, the sensitivity is lower when the window is centrally placed in the speckle field than when the window is placed where the intensity level drops abruptly, i.e. where an intensity cliff is present, as shown Fig 2(a). However, when the window size is increased, the sensitivity can be improved for the centrally placed window. This is because this larger window covers the intensity cliff even if it is placed at the center of the speckle field, and the net power exchange at the edges of the window is sufficient, leading to higher signal amplitude.

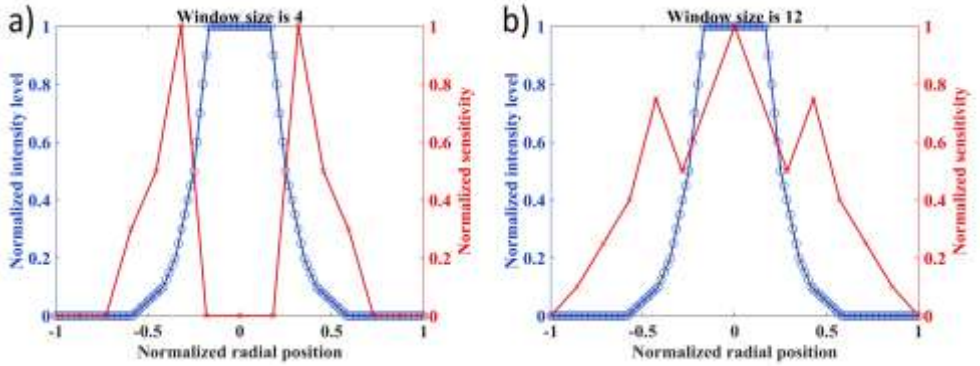

Fig. 2. The normalized speckle intensity distributions (blue) and corresponding sensitivity curves (red) of the spatial filtering windows at different locations with window sizes of: a) 4 rings, and b) 12 rings. Each circle in the blue curve represents a spatial ring in the image plane.

3. Experiment and results

The experiment setup used to investigate the response of speckle sensor to external perturbation is shown in Fig. 3. A pigtailed laser diode (Thorlabs LP642-SF20) operating at 642nm with an output power of 12mW (maximum output 20mW) was used. An FC/PC connector connected the laser-diode and the MMF. The MMF had an NA of 0.39 and a core diameter of 200μm. There were 100 turns of fiber wrapped around the piezoelectric transducer, approximate 8.8m in total length. A function generator (RIGOL DG4162) generated a 5Hz $1V_{pp}$ sine wave, which was subsequently amplified by a high voltage amplifier (Pintech HA-405) to $100V_{pp}$. An objective lens with an NA of 0.65 was used to collimate the light at the output of the MMF, and the output was imaged by a CCD camera (1024×1280 pixels, GigaView SVSI). The exposure time was chosen as 9μs to avoid CCD saturation and to ensure sufficient brightness. The frame rate was 500Hz and the recording time was 2 seconds, so that 1000 image frames were captured in each measurement.

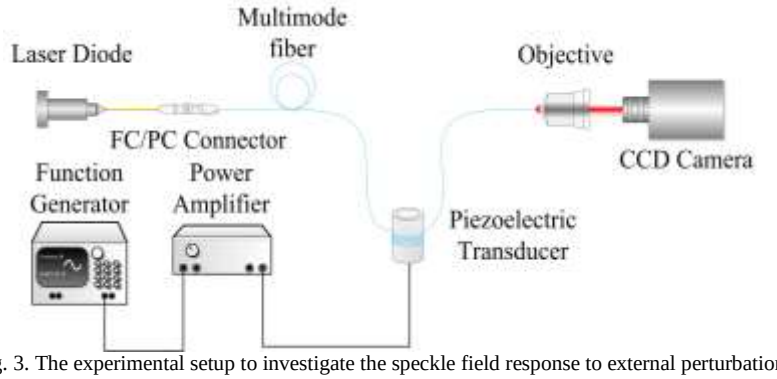

Fig. 3. The experimental setup to investigate the speckle field response to external perturbation

The captured frames of the speckle field were all firstly sectioned to sub-images. For example, Fig 4(a) showed one captured frame of the speckle field. This frame was subsequently sectioned into 64×80 sub-images corresponding to spatial filtering windows of 16×16 pixels in Fig. 4(b). Each window was labeled by its row and column numbers.

Before any further analysis, the Nyquist imaging criterion for speckle imaging was verified to ensure that there were at least 2 pixels for each one-dimensional speckle [31,32]. Here we defined the pixel with the highest intensity among all other pixels in a speckle as the local intensity maxima of this speckle. Subsequently the number of local intensity maxima was counted to estimate the number of speckles. Then, based on the number of pixels occupied by the speckle field, we estimated that there were 17 to 19 pixels in each speckle, which satisfied the Nyquist imaging criterion.

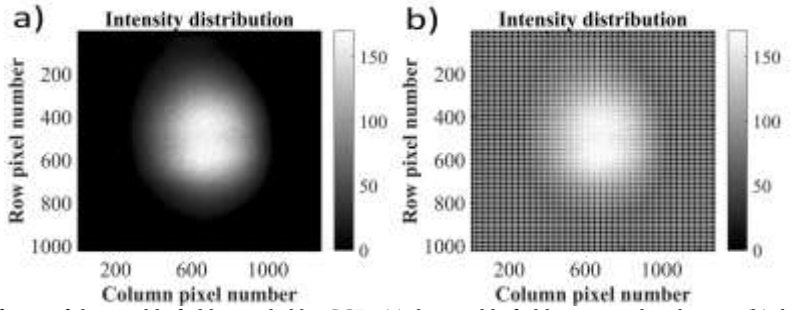

Fig. 4. One frame of the speckle field recorded by CCD. (a) the speckle field intensity distribution; (b) the same frame sectioned into 64×80 sub-images corresponding to spatial filtering windows of 16×16 pixels.

Fig. 5 shows the total intensity of three representative windows at the periphery, the middle, and the inner regions along the radial direction of the speckle field, i.e. the sub-images (33,18), (33,27), (33,36). The total intensity was calculated by adding the intensities of all the pixels in the selected window. Clearly, when there was no perturbation applied to the MMF, the total intensity of the windows remained as a constant except for some background noise, due to such as the inherent mode coupling and the noise of CCD camera. However, when the 5Hz perturbation was applied on the MMF, the total intensity varied as a result of the perturbation. The signal contained both the 5Hz component and its harmonics. This was because the coefficient χ in Eq. (10) contains the harmonic components of the applied perturbation [24,25].

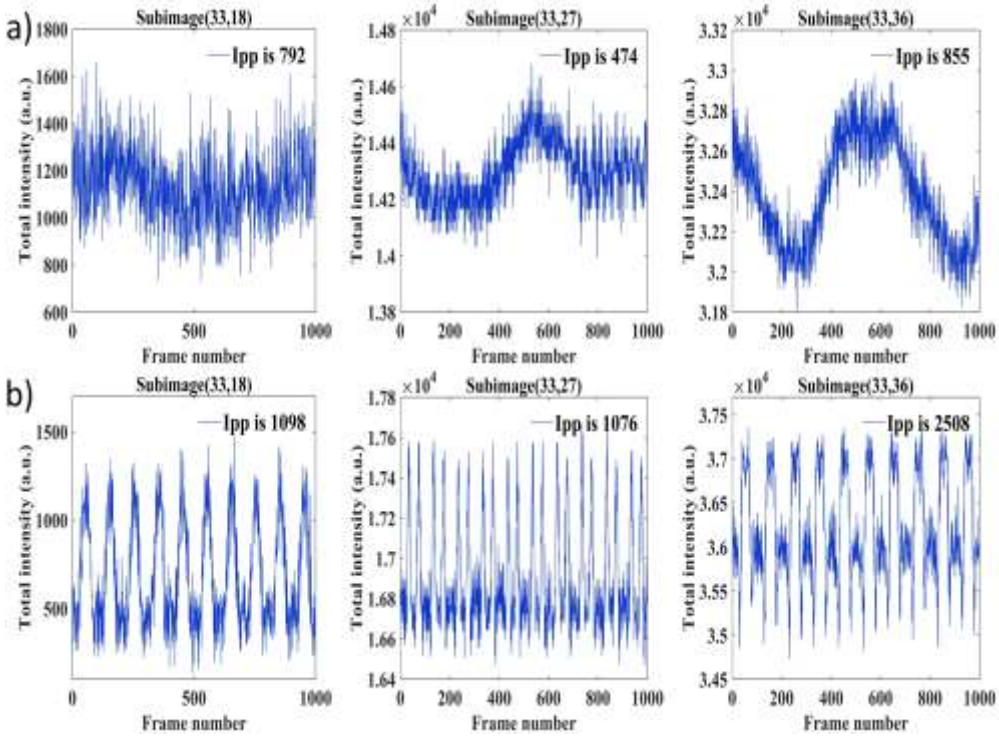

Fig. 5. The total intensity of the selected speckle sections by different windows. (a) Background noise when the piezoelectric transducer was not activated; (b) the response when the $100V_{pp}$ 5Hz sine wave was applied to the piezoelectric transducer. I_{pp} represents the intensity level peak to peak, which determines the sensitivity.

The I_{pp} maps and the corresponding AC signal waveforms are shown in Fig. 6. These plots were obtained using the following procedure. The speckle image was firstly sectioned to a number of small windows, as described previously. As 1000 frames of the speckle field under external perturbation were acquired, we calculated the total intensity sum of each window in each frame and therefore obtained 1000 intensity values (over 1000 frames) for each window. By plotting these intensity values, an AC waveform of each window for 1000 frames was obtained. The I_{pp} value for each window was then calculated based on the waveform. It can be seen for the windows of 16×16, 32×32, 64×64 pixels, the I_{pp} was lower at the center of the speckle field and then increased when it was away from the center. For the window of 256×256 pixels, the I_{pp} was higher at the center of the speckle field. It should be noted that a larger window is not always desirable, even though the I_{pp} value can be higher sometimes. A larger window introduced higher noise level as shown in Fig 6. The I_{pp} waveforms of windows at 16×16, 32×32 and 64×64 pixels displayed reasonable signal to noise levels. However, for the windows of 128×128 and 256×256 pixels, the I_{pp} waveforms became very noisy. If the intensity level of the whole speckle field was summed, no signal was observed in Fig 6(f). This can be explained according to the light power conservation. Based on the above analysis, we can conclude that both the size and the location of the spatial filtering window need to be carefully chosen in order to optimize the sensing performance.

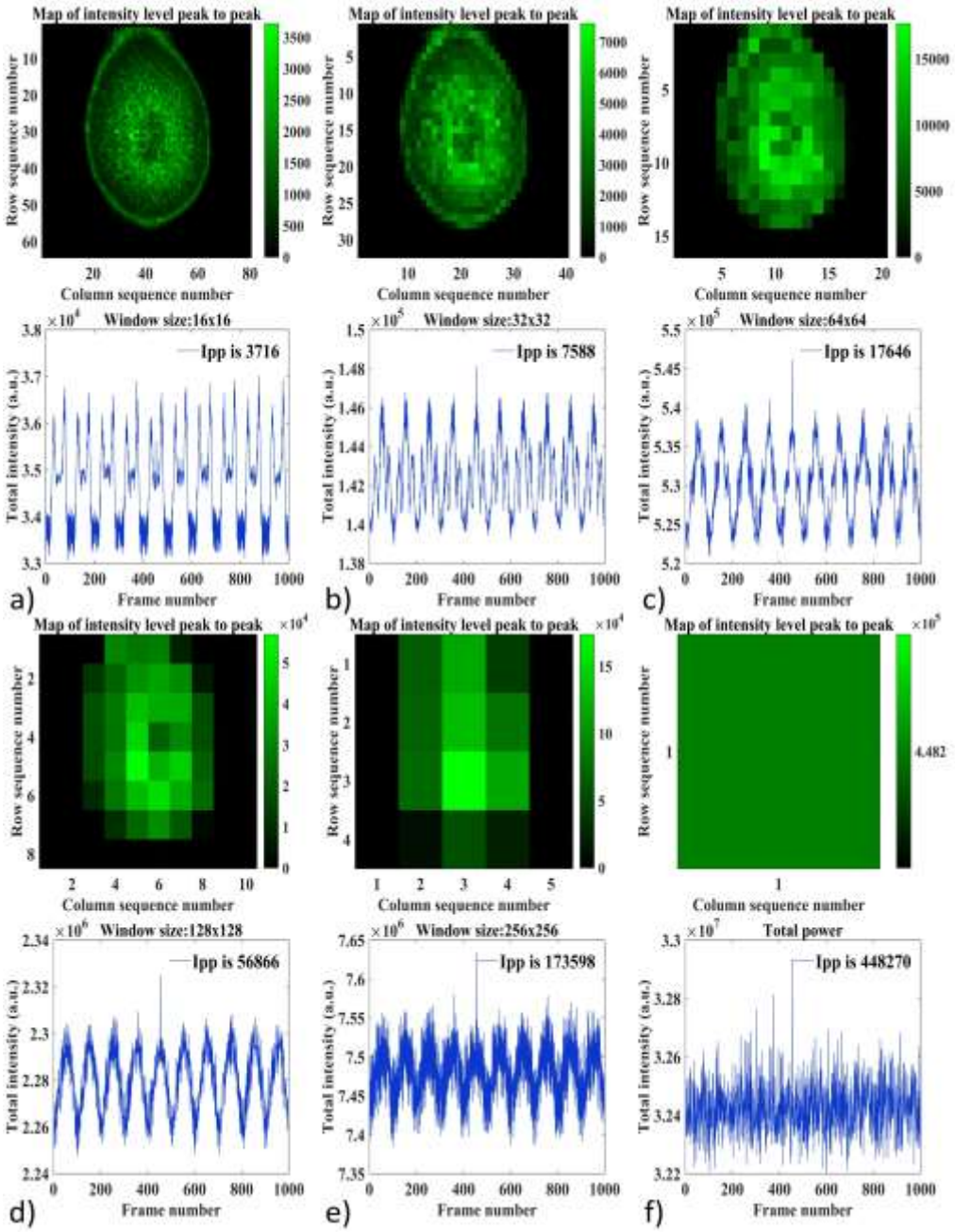

Fig. 6. Maps of I_{pp} and corresponding signal waveforms with the largest I_{pp}. The speckle field was sectioned into sub-images corresponding to the filtering window sizes of a)16×16, b)32×32, c)64×64, d)128×128, e) 256×256, and f) 1024×1280. The signal waveforms with the largest I_{pp} were given for, a) sub-image (32,35), b) sub-image (18,18), c) sub-image (9,9), d) sub-image (5,5), e) sub-image (3,3), and f) the whole image. For each sectioning window, the total intensities of 1000 frames were firstly calculated to obtain the waveforms and the I_{pp} values.

In summary, the results agree well with our theoretical analysis conducted in the Section 2. The sensitivity depends on the location and the size of the filtering window which covered the sectioned speckle field of different intensity profile. To further demonstrate this, the normalized intensity profile of the 512th row is shown using the blue curve in Fig. 7. The corresponding sensitivity to this intensity profile was calculated using Eq. (10). As discussed

previously, the values of α and β were set to 1 by assuming the window completely covered the edge cylindrical modes. Based on the number of pixels occupied by the speckle field and the number of cylindrical modes estimated according to the formula given in [21], each pixel was estimated to correspond to 1 to 2 projected cylindrical modes on the image plane. In this case, we used the intensity difference between neighboring pixels as the approximated values for intensity difference ($\Delta_{(i)(i+1)}$) between the neighboring modes. The measured sensitivity (the green curve) of the windows that covers the blue intensity profile was obtained by using the I_{pp} maps of Fig. 6(a) and Fig. 6(e). The measured sensitivity and calculated sensitivity using Eq. (10) agree with each other. It can be clearly seen in Fig. 7 that for the window of 16×16 pixels, the calculated sensitivity is higher at the location where the intensity level abruptly dropped. For the window of 256×256 pixels, the sensitivity is higher at the center. This agrees with the discussion in Section 2, because this centrally-placed window covers the intensity cliff, and therefore sufficient net power exchange is detected at the edge of the window.

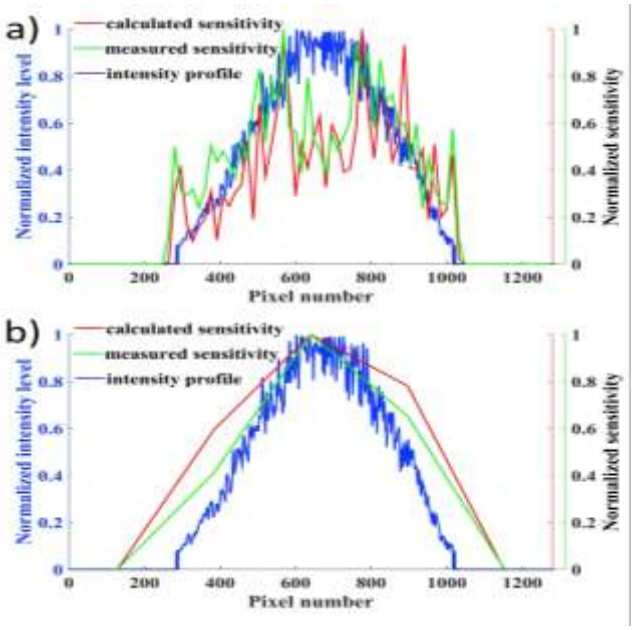

Fig. 7. Intensity profile of pixels at 512th row and the sensitivity of corresponding windows of (a) 16×16 pixels, and (b) 256×256 pixels. The intensity profile is the blue curve. The green curve is the measured sensitivity (I_{pp}) of windows which covered the 512th row, obtained from the maps in Fig. 6(a) and Fig. 6(e). The red curve represents the calculated sensitivity based on the intensity profile using Eq. (10).

According to Nyquist sampling criterion, the CCD camera used needs to have a sampling rate at least twice the frequency of the signal [33]. However, most CCD cameras have limited frame rates, which is not suitable for high-speed signal measurement. Therefore, we built a photodetector-based sensing system, as shown in Fig 8.

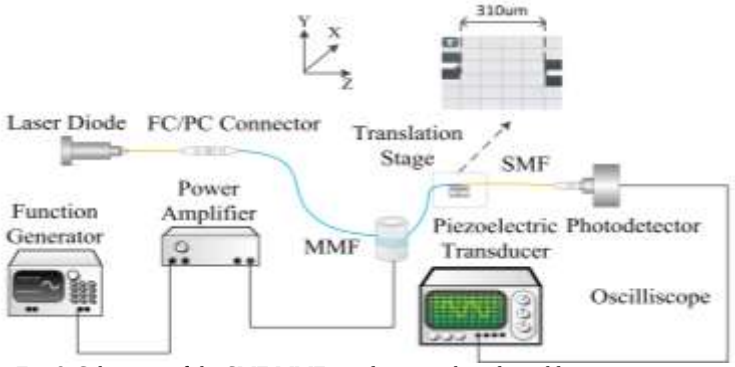

Fig. 8. Schematic of the SMF-MMF misalignment-based speckle sensing system

The laser diode, the function generator, and the amplifier were the same as those used in Fig. 3. The MMF had a core diameter of 50μm and a NA of 0.22. The SMF used as the filtering window and the laser fiber pigtail had a 0.10 NA and a mode field diameter of 4.3 – 4.6μm. This SMF was connected to a Si photodetector (Thorlabs PDA36A) by a FC/PC connector. The translational stage of a fusion splicer was used to adjust the alignment between the SMF and the MMF manually with a translational resolution of 6μm. In order to have enough measurement points, the speckle image projected to the input plane of the SMF should be as large as possible so that the SMF can be misaligned with respect to the MMF at several positions. Therefore, the axial distance between the SMF and the MMF should be as large as possible. In our experiment, the axial distance between the SMF and the MMF was adjusted to be 310μm, which was the maximum distance allowed by the translational stage. Then, the measurements were conducted with the SMF-MMF misalignment being 6μm, 12μm, 18μm, 24μm, 30μm, 36μm and 42μm along the Y direction. During the alignment procedure, the output power was monitored by a power meter (Thorlabs PM20A). Then, a 100V_{pp} 50Hz sine wave was applied to the piezoelectric transducer, and the signal response was monitored by the photodetector and displayed on the oscilloscope.

The coupled power from MMF to SMF and the voltage peak to peak (V_{pp}) of the detected signals are shown in Fig 9. The corresponding specific signal curves are shown in Fig 10.

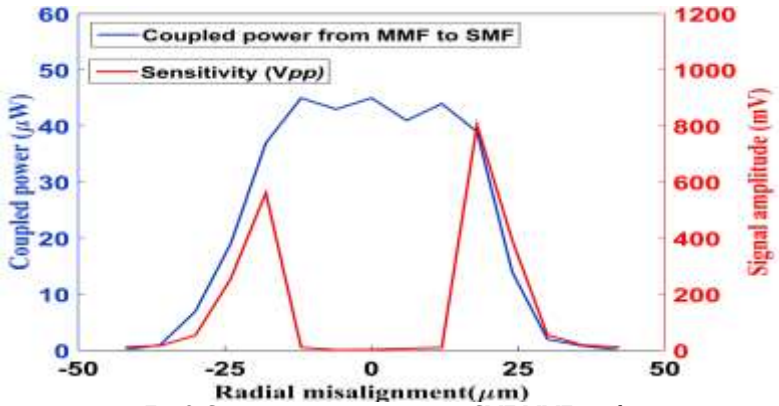

Fig. 9. Sensitivity improvement using SMF-MMF misalignment

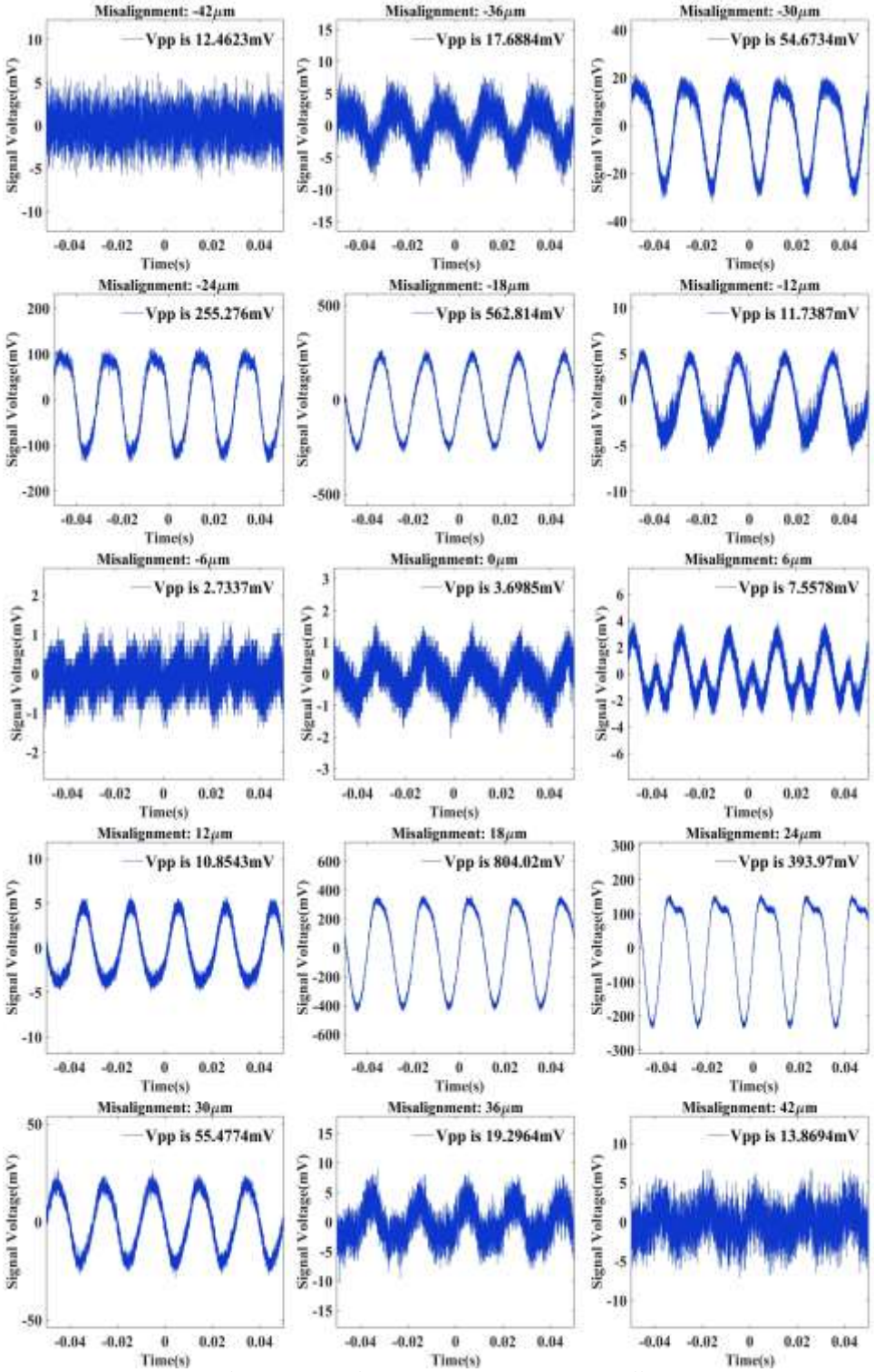

Fig. 10. Detected signal waveforms when the filtering SMF was misaligned to different positions with respect to the sensing MMF.

It can be seen clearly that the measured curves in Fig. 9 agree well with the expectation given in Fig. 2. The sensitivity was very low when the SMF was located at the center of the MMF, with the best signal amplitude of 11.7mV. When the SMF was moved to the position where the power level abruptly dropped, a significant sensitivity improvement can be observed. The highest signal amplitude measured in our experiment was 804mV. This corresponded to a sensitivity enhancement of 80 folds. Therefore, it proved that the sensitivity of the speckle sensor depends on the intensity profile of the MMF modes. An appropriate designed window can be used to enhance the sensitivity of the speckle sensor.

4. Conclusion

In this paper, we investigated both theoretically and experimentally the sensitivity enhancement of a speckle sensor by adjusting the spatial filtering window. A simple theoretical model based on mode-coupling equations was developed to describe the influence of the spatial filtering window on sensitivity. We demonstrated that the sensitivity of the speckle sensor highly depends on the efficiency of net power exchange of the spatial filtering window that covers different spatial modes. Particularly, a high sensitivity can be obtained if the neighboring modes at the edges of the window have a large power difference. In this way, a more efficient net-power exchange to the filtering window can be achieved, thereby leading to a higher sensitivity. We used two speckle sensor experiment configurations to verify our theory. The sensitivity improvement up to 80-fold was achieved in our experiment and good agreements were found between the theoretical analysis and experimental results. Our results lead to the conclusion that both the location and the size of the spatial filtering window are critical when designing a fiber-optic speckle sensor. This should be useful for future fiber-optic speckle sensor theory and design.

Acknowledgments

The authors sincerely acknowledge the financial support from the National Science Foundation of China (Grant No. 51577149), and State Key Laboratory of Electrical Insulation and Power Equipment (Grant No. EIPE14117). This work was supported by the Engineering and Physical Sciences Research Council [grant number EP/L022559/2].